



ELSEVIER

Contents lists available at ScienceDirect

Comptes Rendus Physique

www.sciencedirect.com



The *Comptes rendus de l'Académie des sciences* throughout history / Les *Comptes rendus de l'Académie des sciences* à travers l'histoire

Henri Bénard and pattern-forming instabilities



Henri Bénard : la découverte des structures dissipatives hors de l'équilibre

Stéphan Fauve

Laboratoire de physique statistique, École normale supérieure, PSL Research University; UPMC, Sorbonne Universités; Université Paris-Diderot, Sorbonne Paris-Cité; CNRS, 24, rue Lhomond, 75005 Paris, France

ARTICLE INFO

Article history:

Available online 21 November 2017

Keywords:

Hydrodynamic instabilities
Patterns
Dissipative systems

Mots-clés:

Instabilités hydrodynamiques
Structures
Systèmes dissipatifs

ABSTRACT

The first quantitative experimental study of thermal convection has been performed by Henri Bénard, who presented his results in two articles published in the *Comptes rendus* in 1900. After describing the first experiments of Bénard and the ones he performed later with his students, we discuss some theoretical steps that led to the full understanding of Bénard's experiments more than fifty years later. We then shortly review some more recent aspects of pattern-forming instabilities that are directly related to the experimental work conducted by Bénard and his students.

© 2017 Académie des sciences. Published by Elsevier Masson SAS. This is an open access article under the CC BY-NC-ND license (<http://creativecommons.org/licenses/by-nc-nd/4.0/>).

R É S U M É

La première étude expérimentale quantitative de la convection thermique a été réalisée par Henri Bénard, qui a publié ses premiers résultats dans deux notes aux *Comptes rendus* en 1900. Après avoir décrit les premières expériences de Bénard, puis celles effectuées par ses étudiants, nous mentionnons les travaux théoriques qui ont permis d'aboutir à une compréhension correcte des expériences, plus de cinquante ans plus tard. Nous passons ensuite en revue des résultats plus récents sur les structures spatiales engendrées par instabilités qui sont en relation avec les travaux expérimentaux de Bénard et de ses étudiants.

© 2017 Académie des sciences. Published by Elsevier Masson SAS. This is an open access article under the CC BY-NC-ND license (<http://creativecommons.org/licenses/by-nc-nd/4.0/>).

1. Introduction

Pattern-forming instabilities in fluid mechanics or in other nonlinear systems driven far from equilibrium are usually related to a transition from a spatially homogeneous (often motionless) state, to one varying periodically in space or time. Thermal convection in a horizontal layer of fluid subjected to a temperature gradient, referred to as Rayleigh–Bénard convection, is a canonical example of pattern-forming instability. It is commonly observed in a layer of fluid heated from below or cooled from above due to evaporation. The flow takes the form of a pattern of convection cells known as Bénard's cells.

E-mail address: fauve@lps.ens.fr.

<https://doi.org/10.1016/j.crhy.2017.11.002>

1631-0705/© 2017 Académie des sciences. Published by Elsevier Masson SAS. This is an open access article under the CC BY-NC-ND license (<http://creativecommons.org/licenses/by-nc-nd/4.0/>).

The appearance of periodic structures in this system driven externally by a forcing homogeneous in space and constant in time, corresponds to a bifurcation, characterized by one mode that becomes unstable as the temperature difference across the fluid layer is increased.

The first quantitative experimental study of thermal convection was carried out by Henri Bénard, who published his first results in two articles in the *Comptes rendus de l'Académie des sciences* in 1900 [1,2]. Other hydrodynamic instabilities were known at the time, but concerned the amplification of waves. In 1831, Faraday observed that standing surface waves can be generated by vertically vibrating a fluid layer [3]. The Kelvin–Helmholtz instability, i.e. waves amplified by a shear flow at the interface between two fluids of different densities, was also observed and understood [4]. Bénard performed the first experimental studies of a stationary instability in a dissipative system and deeply influenced this field of research during the following century. In addition, he was one of the first to tackle a fluid mechanics problem using state-of-the-art experimental techniques of his time to perform accurate measurements. Fluid dynamics at the time of Bénard was indeed often based on qualitative observations that either motivated theoretical approaches or were used afterwards to test the result of an analytical calculation. This quest of experimental precision has motivated Bénard to consider problems related to pattern-forming instabilities that have been addressed and solved years later. In his first experiments, he explained how the shape of the generated pattern can be affected by local inhomogeneities and by lateral boundaries, and he tried his best to avoid pattern selection by lateral boundaries. Together with his student Avsec [5], he reported that although there exists an optimal wavelength for pattern formation, patterns with other wavelengths in a wide range around the optimum can be generated depending on initial conditions or on external perturbations. They also reported that patterns with a wavelength far from the optimum are unstable. As we will discuss below, these problems of pattern selection by nonlinear interactions between different unstable modes and of selection of the pattern wavelength have been considered and solved decades later. Most of them have been reviewed in the 1970s or in the 1980s [6–10].

2. Henri Bénard

A detailed biography of Henri Bénard has been written by J. E. Wesfreid a few years ago [11]. We give below only a short summary. Henri Bénard was born in 1874 at Lieurey, a village of Normandy. After finishing elementary school nearby his birthplace, he moved to Paris where he studied at the Lycée Louis le Grand. In 1894, he entered Ecole normale supérieure in Paris where he was a classmate of the physicist Paul Langevin and of the mathematician Henri Lebesgue. Henri Bénard did his PhD at the ‘Collège de France’, where he started working in 1897 as an assistant of Eleuthère Mascart and Marcel Brillouin. After a first study in optics, he began to work in fluid mechanics under the influence of Brillouin. Using several optical methods, he studied the generation of convection cells in a horizontal layer of fluid heated from below. He published his first results in two notes in the *Comptes rendus de l'Académie des sciences* [1,2] in 1900 and defended his thesis in 1901. He published a longer paper on his results the same year [12], where the experimental techniques he used were presented in great detail. After his PhD, Bénard was appointed assistant-professor at the Faculty of Sciences in Lyon. He began to work on the deformation of liquid surfaces under the influence of a flow with vorticity. He designed an experimental facility to study vortex shedding in the wake of an obstacle [13], another phenomenon that has been named after him and Theodore von Kármán, the Bénard–von Kármán street. He used cinematography as a means of observation and measurement several decades before it became a commonly used experimental method [14]. In 1910, Bénard was appointed professor at the University of Bordeaux. During the First World War, he was affected to a commission for military applications. He improved the refrigeration wagons transporting meat, worked on the detection of the wakes of ships and submarines, built a periscope using polarized light and panoramic glasses with cylindrical lenses to enlarge the image in one direction. In 1922, Bénard moved from Bordeaux to Paris where he became assistant-professor at Sorbonne University and then full professor in 1926. He was in charge of the laboratory of experimental fluid dynamics created in 1929 in collaboration between the Sorbonne University and the Ministry of Aeronautics. Besides industrial applications of fluid dynamics, Bénard was interested in the topic now called geophysical and astrophysical fluid dynamics. He is one of the first to have shown that laboratory experiments can give insights into astrophysical or meteorological phenomena, although they occur at much larger scales. His last papers together with Douchan Avsec discuss experimental models for solar granulation and dynamics of clouds [5].

3. Bénard's experiments on convection

Bénard decided to study thermal convection during the second year of his PhD work, after observing the motion of graphite particles in molten paraffin [11]. In his first note on the subject [1], he quotes two earlier qualitative observations of convection. It is likely that several others exist, as for instance James Thomson quoted by Rayleigh [15], but Bénard is the first to have designed a careful experiment in order to perform a quantitative study of thermal convection. The configuration he studied, now referred to as Rayleigh–Bénard convection, consists of a horizontal layer of fluid heated from below. Most fluids being less dense as their temperature increases, the resulting density stratification with light fluid layers below denser ones generates an instability above a critical temperature difference when the buoyancy force overcomes the stabilizing effects of viscosity and heat diffusivity. The motionless state is then replaced by an array of convection cells (see Fig. 1).

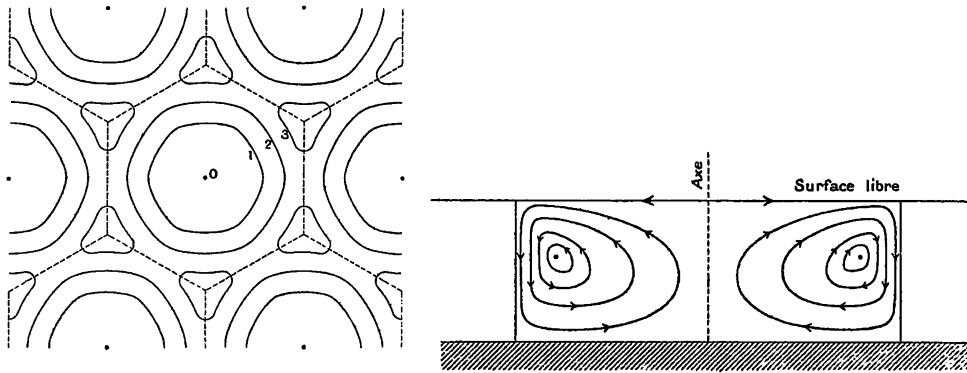


Fig. 1. Bénard's drawings from references [1,2]. (Left) Sketch of the convection pattern seen from above. (Right) Sketch of the flow in a cut of an hexagonal cell. The hot fluid rises along the central axis of the cell, gets colder after circulating along the upper free surface, moves downward along the edges of the hexagonal cell and gets hot after moving along the heated bottom plate.

Bénard emphasized that particular care should be taken in order to observe ordered stationary patterns of hexagons. First, he insists on the homogeneity in the horizontal plane of the experimental configuration. Second, he mentioned that if a fluid of low viscosity is used or if the heating power is too large, the patterns are disordered and time dependent. In the case of stationary patterns, he wrote that the most perfect ones consist of hexagons. He sketched the streamlines of the flow within each hexagonal cell as displayed in Fig. 1 (right). The hot fluid rises along the central axis of the cell, gets colder after circulating along the upper free surface, moves downward along the edges of the hexagonal cell and gets hot after moving along the heated bottom plate. Bénard noted that for a given fluid, the hexagonal pattern is characterized by a unique wavelength that is roughly proportional to the depth of the fluid layer (within 10%) and depends on the heat flux. He emphasized that all hexagons have the same area within 1% and that their edges along the three directions of the pattern stay parallel within 2 or 3° throughout the whole sample. He concludes by emphasizing the analogy with a crystal and wrote: “this is the first example of a physical phenomenon for which uniform conditions in the horizontal plane generate a perfect cellular structure.”

Bénard described his experimental techniques in detail in a longer paper [12]. After noticing that convection can occur at room temperature with volatile liquids such as ethanol, diethyl ether, or benzene because of the temperature gradient generated by evaporation, but does not provide a well-controlled experimental configuration, Bénard decided to work with non-volatile liquids. He also observed that stationary convection is difficult to obtain when the thickness of the fluid layer is too large and chose to work with layer heights of the order of a millimeter. His first experimental set-up is sketched in Fig. 2. A thick metallic plate (PP) is heated at 100 °C by a flow of steam, the circulation of steam being designed in an axisymmetric way in order to provide a homogeneous heating. The upper part of the plate is machined such as to have a cylindrical side wall, 10 mm in height, containing the fluid. In order to have a liquid with low volatility at this temperature, Bénard chose spermaceti oil or cetyl palmitate. Because of its high viscosity and of the small thickness of the layer, an intense heating was required to generate convection, but it was easy to observe spatially ordered stationary patterns even well above the convection threshold. Bénard stressed the need for a large enough plate in order to avoid the effect of lateral boundaries on the convection patterns. Although he noted that a solid upper boundary would lead to a more symmetric configuration, he chose to work with an upper free surface in order to be able to use several optical measurement techniques.

Bénard measured the thickness of the layer of millimeter size using the device (OB) displayed in Fig. 2. It consists of a lever rotating about an horizontal axis (O) and holding a needle (A). Looking at the needle and at its image reflected by the liquid surface using a telescope with high magnification in grazing incidence, Bénard used the screw (K) to make the needle and its image coincide and measured the vertical displacement of the cross (B) using a cathetometer. Repeating the same procedure without liquid, using the image of the needle reflected by the polished steel bottom plate, he deduced the thickness of the fluid layer with a precision of a few microns.

He first used different types of particles in order to follow the streamlines and to measure the flow velocity of the order of a few mm/s. He managed to measure its variation from one streamline to the other, measured the surface velocity using light particles and the velocity close to the bottom boundary using denser particles. He determined the heat flux crossing the liquid layer by measuring the temperature drop within the bottom boundary and found that the convection velocity increases with the heat flux. He also noticed that, in the long-time limit, particles denser than the fluid agglomerate on the bottom boundary in the center of each hexagonal cell, thus generating a perfect triangular pattern.

Bénard also used several optical techniques for more precise measurements of the convection pattern. He observed that the free surface of the fluid cannot be flat due to variation of pressure related to surface tension and horizontal flow. Although of order of 0.5 μm in the case of Bénard's experiments, these deformations, reproducing the flow pattern, could be observed by light reflection in oblique incidence by the free surface. Bénard first used a method designed by Foucault to test mirrors of telescopes. He observed the image of a grid by the free surface and relates the deformation of the image

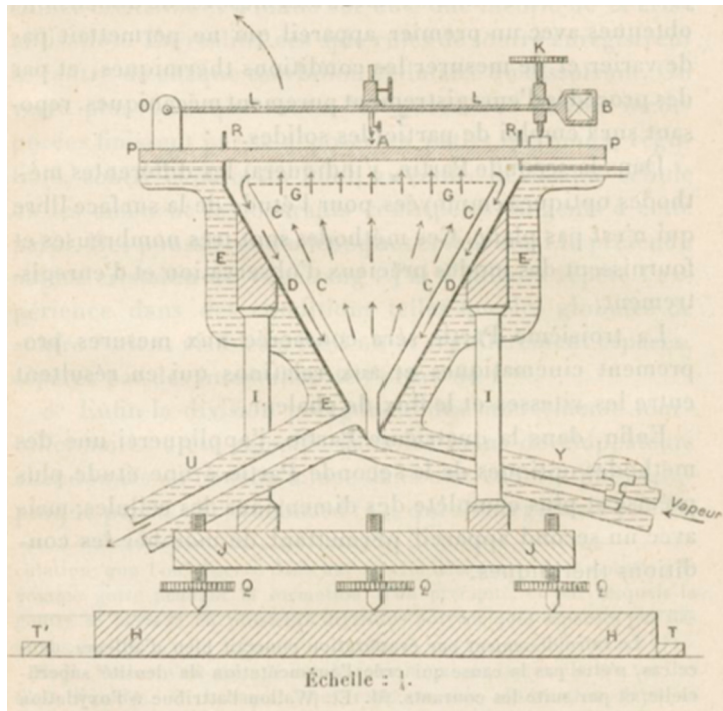


Fig. 2. Bénard's sketch of his first experimental set-up from reference [12].

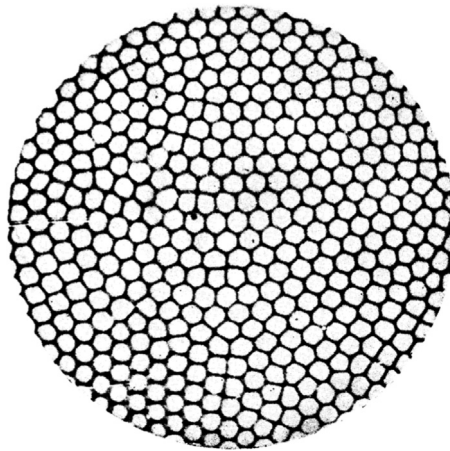


Fig. 3. One of Bénard's photograph of the convection pattern seen from above in reference [5].

of that grid to the curvature of the free surface. This method however proved to be too sensitive far from the convection threshold. He then observed interference fringes generated between the free surface and a horizontal glass plate above the free surface and counted them to estimate the variation of the height of the free surface within an hexagonal cell. The height is minimum at the center of each hexagon, whereas the maximum is reached on the vertices. The midpoint between the two vertices on each edge is a saddle point. The contour lines displayed in Fig. 1 (left) have been drawn according to these height measurements. He also used the interference fringes generated between the free surface and the surface of the bottom plate after polishing it in order to determine the isotherms within the fluid. Bénard took many photographs of the convection patterns and used them for a quantitative study of the geometry of the patterns and their dependence on the thickness of the layer or on the heat flux. He considered both the light reflected by the free surface and the one refracted through the fluid layer. The second configuration was achieved by polishing the surface of the bottom plate. In that case, the light reflected by the bottom plate and being refracted through the fluid layer was much more intense than the light directly reflected by the free surface. One of these photographs is displayed in Fig. 3.

4. First studies motivated by Bénard's experiments on convection

4.1. Rayleigh's linear stability analysis

Lord Rayleigh presented the first theoretical explanation of Bénard's results in 1916 [15]. His paper begins by acknowledging Bénard: "The present is an attempt to examine how far the interesting results obtained by Bénard in his careful and skillful experiments can be explained theoretically." Rayleigh used the Boussinesq approximation, which consists in neglecting the variation of the fluid parameters with temperature, in particular the density, except where they are multiplied by the acceleration of gravity in the equation of motion for the velocity [16]. The heat generated by viscous friction as well as compressible terms in the energy equation are also neglected. The Boussinesq equations for the velocity $\mathbf{v}(\mathbf{r}, t)$, pressure $p(\mathbf{r}, t)$ and temperature $T(\mathbf{r}, t)$ fields are:

$$\nabla \cdot \mathbf{v} = 0 \quad (1)$$

$$\rho_0 \left[\frac{\partial \mathbf{v}}{\partial t} + (\mathbf{v} \cdot \nabla) \mathbf{v} \right] = -\nabla p + \rho_0 \nu \nabla^2 \mathbf{v} - \rho(T) g \hat{\mathbf{z}} \quad (2)$$

$$\frac{\partial T}{\partial t} + \mathbf{v} \cdot \nabla T = \kappa \nabla^2 T \quad (3)$$

where g is the acceleration of gravity, $\hat{\mathbf{z}}$ is the unit vector along the vertical direction, ν is the fluid kinematic viscosity and κ is the heat diffusivity; ρ_0 is the fluid density at a reference temperature, and T is the temperature difference from that reference. Thus,

$$\rho(T) \simeq \rho_0(1 - \alpha T) \quad (4)$$

Defining θ as the temperature fluctuation from the heat-conducting profile,

$$T = T_0 - \frac{\Delta T}{d} z + \theta \quad (5)$$

where ΔT is the temperature difference across the layer of height d , and using d , d^2/κ and ΔT as scales for length, time and temperature, one gets

$$\nabla \cdot \mathbf{v} = 0 \quad (6)$$

$$\frac{\partial \mathbf{v}}{\partial t} + (\mathbf{v} \cdot \nabla) \mathbf{v} = -\nabla \pi + P \nabla^2 \mathbf{v} + RP\theta \hat{\mathbf{z}} \quad (7)$$

$$\frac{\partial \theta}{\partial t} + \mathbf{v} \cdot \nabla \theta = \mathbf{v} \cdot \hat{\mathbf{z}} + \nabla^2 \theta \quad (8)$$

where π stands for the terms that can be put in the form of a gradient, $P = \nu/\kappa$ is the Prandtl number, and $R = g\alpha\Delta T d^3/\nu\kappa$ is the Rayleigh number. These two dimensionless numbers, together with the boundary conditions, characterize the convection problem in the Boussinesq approximation. The Prandtl number is the ratio of the time scales of the two diffusive processes involved in convection, heat diffusion, and momentum diffusion. Depending on the microscopic mechanisms of transport, the Prandtl number varies on many orders of magnitude in different convective flows of interest. The Rayleigh number represents the ratio of the acceleration $g\alpha\Delta T$ related to buoyancy to the stabilizing effects of kinematic viscosity and heat diffusivity.

Rayleigh considered the case of horizontal boundaries of infinite extent at $z = 0$ and $z = 1$ (in dimensionless form). He assumed that the boundaries have a much larger heat conductivity than the one of the fluid, thus the temperature perturbation vanishes, $\theta(x, y, 0, t) = \theta(x, y, 1, t) = 0$. In addition, he assumed that the boundaries are stress-free, i.e. they do not exert a frictional force on the fluid, $\partial \mathbf{v}_h / \partial z(x, y, 0, t) = \partial \mathbf{v}_h / \partial z(x, y, 1, t) = 0$, where \mathbf{v}_h is the horizontal component of the velocity field. Using the incompressibility condition, this gives $\partial^2 w / \partial z^2(x, y, 0, t) = \partial^2 w / \partial z^2(x, y, 1, t) = 0$ together with the condition on the vertical component w of the velocity field, which should vanish at the boundaries, $w(x, y, 0, t) = w(x, y, 1, t) = 0$. Stress-free boundary conditions could be a fair approximation for the upper boundary in contact with air provided one could neglect surface deformation and surface tension. It is not correct for the bottom solid boundary where all the components of the velocity field should vanish. However, stress-free boundary conditions are the only ones that allow a fully analytic calculation.

Linear stability analysis of the motionless state, $\mathbf{v} = 0$ with the linear temperature profile given by (5) is performed by assuming small perturbations of velocity \mathbf{v} and temperature θ , and therefore neglecting all the nonlinear terms in Eqs. (7), (8). We first eliminate the pressure field by applying the operators curl and curl curl to the momentum Eq. (7) and we get the evolution equations for the vertical vorticity, ζ , and the vertical velocity, w , by projecting on the vertical axis. At the linear stage, we observe that the vertical vorticity decouples and obeys a diffusion equation. Thus, the vertical vorticity modes can be ignored in the linear stability analysis. The equation for the vertical velocity w is

$$\frac{\partial}{\partial t} \nabla^2 w = P \nabla^4 w + RP \nabla_h^2 \theta \quad (9)$$

where ∇_h^2 stands for the Laplacian operator in the horizontal plane. We get from the linearized heat Eq. (8)

$$\frac{\partial \theta}{\partial t} = w + \nabla^2 \theta \quad (10)$$

Eliminating θ , we get from (9), (10)

$$\left(\frac{\partial}{\partial t} - \nabla^2 \right) \left(\frac{\partial}{\partial t} - P \nabla^2 \right) \nabla^2 w = RP \nabla_h^2 w \quad (11)$$

From the requirement of spatial periodicity in the horizontal plane, we consider a normal mode of w under the form

$$w(x, y, z, t) = W(z) \exp[i \mathbf{k} \cdot \mathbf{r} + \sigma t] \quad (12)$$

where \mathbf{r} is the position vector in the horizontal plane, and \mathbf{k} is the pattern (horizontal) wave vector. Boundary conditions together with equations (9), (10) require that W and all its even derivatives vanish for $z = 0$ and $z = 1$. It follows that

$$W(z) = W_0 \sin(n\pi z) \quad \text{with } n = 0, 1, \dots \quad (13)$$

Using (11), (10) together with (12), (13) we obtain the dispersion relation for the growth-rate σ of the normal mode of wavenumber k

$$\sigma^2 + q_n^2(1 + P)\sigma + \left(Pq_n^4 - \frac{RPk^2}{q_n^2} \right) = 0 \quad (14)$$

where $q_n^2 = k^2 + n^2\pi^2$.

A stationary instability occurs when the constant term in σ of the dispersion relation vanishes and becomes negative. Thus, as the Rayleigh number is increased, a mode with $n = 1$ bifurcates first for $R = R_c(k)$ with

$$R_c(k) = \frac{(\pi^2 + k^2)^3}{k^2} \quad (15)$$

This defines the marginal stability curve on which a mode with $n = 1$ and horizontal wavenumber k has a zero growth rate. The critical Rayleigh number R_c and the critical wavenumber k_c at convection onset correspond to the minimum of the marginal stability curve (15),

$$R_c = \frac{27\pi^4}{4}, \quad k_c = \frac{\pi}{\sqrt{2}} \quad (16)$$

In dimensional form, the most unstable wavelength is therefore $\lambda_c = 2\sqrt{2}d$. For a one-dimensional pattern of convection rolls, the roll diameter is of the order of the height of the layer. Rayleigh's analysis has been performed later for more realistic boundary conditions [17]. As long as the horizontal boundaries (at least one of them) have a heat conductivity much larger than the one of the fluid, no qualitative change is observed. When the heat conductivity of both horizontal boundaries decreases, k_c decreases and vanishes in the limit of thermally insulating boundaries [18].

Slightly above criticality we expand the positive solution σ_+ to the dispersion relation (14) and get the growth-rate of the unstable modes to leading order in $R - R_c$ and $K = k - k_c$,

$$\sigma_+(K, \mu) = \mu - \alpha K^2 + \dots \quad (17)$$

with

$$\mu = (\pi^2 + k_c^2) \frac{P}{1 + P} \frac{(R - R_c)}{R_c} \quad (18)$$

$$\alpha = (\pi^2 + k_c^2) \frac{P}{1 + P} \frac{1}{2R_c} \left(\frac{\partial^2 R_c}{\partial k^2} \right)_c \quad (19)$$

Therefore, for R larger than R_c , there exists a band of unstable modes with growth rates determined by Eq. (17).

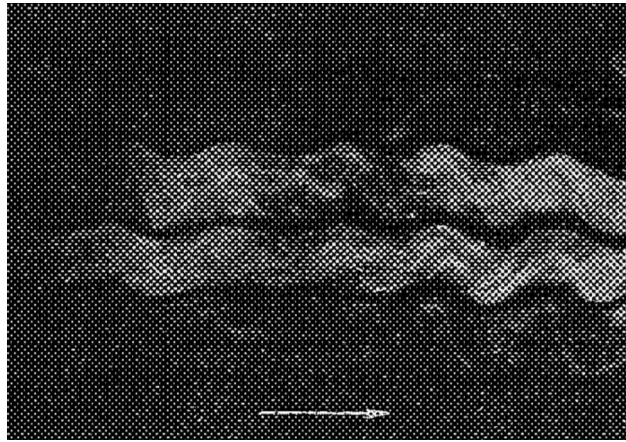


Fig. 4. Avsec's photograph of the instability of parallel convection rolls in air seen from above. The arrow indicates the direction of the forced horizontal flow. Two rolls are visualized by smoke.

4.2. Bénard or Marangoni convection

Bénard became aware of Rayleigh's work only after World War I and Rayleigh's death. He tried to check Rayleigh's quantitative predictions for the most unstable wavelength λ_c and for the convection threshold. He found that λ_c is in good agreement with the wavelength of the pattern observed in his experiments [19]. In contrast, Bénard and others found a strong discrepancy for the convection threshold, the temperature difference in Bénard's experiments being orders of magnitude smaller than the prediction of Rayleigh for the threshold. As said above, Bénard discussed the effect of surface tension on the free surface [12], a phenomenon that was not taken into account by Rayleigh. In 1912, Dauzère, a collaborator of Bénard, studied convection in liquid wax and showed that different patterns can be obtained depending on how the wax was prepared and purified. He considered that these differences result from a modification of the surface tension of liquid wax [20]. In 1935, Volkovski, one of Bénard's students, observed the instability of a liquid layer subjected to a horizontal temperature gradient maintained by the differential heating of the lower boundary and considered that this instability resulted from a surface tension gradient [21]. It was not until 1956 that Block clarified the problem by repeating Bénard's experiments and by showing that it was enough to cover the free surface with a monolayer to suppress convection. On the other hand, he showed that the convection was maintained when the temperature gradient was reversed, the lower boundary being cooler [22]. He concluded that the buoyancy force was not responsible for convection in Bénard's experiments and that the driving mechanism was the surface tension gradient [22]. Finally, in 1958, Pearson performed the linear stability analysis of a horizontal layer of fluid submitted to a vertical temperature difference taking into account surface tension but discarding gravity [23]. The parameters ρ_0 , ν , κ , ΔT , d , $g\alpha$ in Rayleigh's analysis are replaced by ρ_0 , ν , κ , ΔT , d , $-\frac{d\gamma}{dT}$, where γ is the surface tension. There are two independent dimensionless numbers as in Rayleigh's analysis. We can choose the Prandtl number and the Marangoni number $Ma = -\frac{d\gamma}{dT} \frac{d\Delta T}{\rho_0 \nu \kappa}$. Ma/R becoming larger when d decreases, we expect surface tension to become dominant compared to buoyancy in the limit of thin layers.

4.3. Forced convection experiments as a laboratory model for clouds dynamics

The usual explanation put forward for the observation of clouds forming periodic bands is the Kelvin–Helmholtz instability that gives rise to the formation of horizontal striped vortices in a fluid with a strong vertical stratification. In that case, the vortices should be perpendicular to the direction of the flow. After observing in some cases that the direction of the flow can be parallel to the bands formed by clouds, Idrac proposed in 1920 that these structures could be generated by thermal convection in the presence of a forced horizontal mean flow [24]. Several PhD students of Bénard worked on experiments designed to test this explanation [25–27,5]. The experiments were conducted in a horizontal layer of air contained between two solid plates and heated from below. The mean horizontal flow was generated either by pumping air or by the motion of a thin metal plate arranged in contact with the lower wall and driven by rotating cylindrical rollers. Above a critical value of the temperature difference between the horizontal plates, convection rolls, parallel to the direction of the forced flow, were generated. As noticed by the authors, the horizontal flow strongly stabilizes convection rolls parallel to the flow direction. It is interesting to note that Avsec provided the first observation of a secondary instability of convection rolls displayed in Fig. 4. Avsec observed that parallel rolls display a sinuous instability generated either by increasing the temperature difference or by decreasing the velocity of the forced horizontal flow. He wrote that the waviness increases when the temperature difference is increased such that the flow becomes disordered for high temperature differences. He also explained how the parallel rolls can be generated with a fairly wide range of wavelengths, $1.25 < \lambda/d < 5$ by perturbing the horizontal flow using a periodic array of small obstacles. This is the first observation of the existence of a finite range of

possible wavenumbers for patterns generated by a stationary instability at an optimum wavenumber. Avsec observed that these patterns are metastable and that their lifetime becomes small when their wavenumber is far from the optimum [5]. It seems that Avsec discovered the Eckhaus, zigzag or oscillatory instabilities, which have been rediscovered years later. The theory of most of these secondary instabilities of convection rolls has been performed by Busse [9].

5. Pattern-forming instabilities

5.1. Pattern selection

Linear analysis gives the critical Rayleigh number R_c for instability onset and determines the modulus k_c of the critical wave vector \mathbf{k} of the unstable modes. The direction of \mathbf{k} is arbitrary; this orientational degeneracy is obviously related to the isotropy in the horizontal plane. There is also a translational degeneracy that is related to the translational invariance of the layer of infinite horizontal extent. These degeneracies do not result from the linear approximation but from the symmetries of the Rayleigh–Bénard geometry; thus, they will subsist in the nonlinear analysis. On the other hand, there is a pattern degeneracy that results from the linear approximation; indeed, any superposition of normal modes

$$w(\mathbf{r}, z) = \sum_{p=1}^N [A_p \exp(i \mathbf{k}_p \cdot \mathbf{r}) + \bar{A}_p \exp(-i \mathbf{k}_p \cdot \mathbf{r})] \quad (20)$$

with $|\mathbf{k}_p| = k_c$ and where the A_p 's are complex amplitudes, is a solution to the linear problem with a zero growth rate at criticality. \bar{A}_p stands for the complex conjugate of A_p such that w is a real field. The number of non-zero A_p 's, i.e. the shape of the pattern, and their modulus, i.e. the amplitude of the convection velocity, remain indeterminate. For instance, $N = 1$ corresponds to a one-dimensional periodic pattern, i.e. a pattern of periodic stripes or periodic convection rolls, $N = 2$ corresponds to parallelograms or squares if \mathbf{k}_1 is perpendicular to \mathbf{k}_2 , $N = 3$, with the wave vectors \mathbf{k}_1 , \mathbf{k}_2 and \mathbf{k}_3 at 120° on the circle of radius k_c generates a pattern of hexagons or triangles depending on the sum of the phases of each components.

Nonlinear interactions between the modes with different wave vectors generally select one pattern at instability onset and determine the amplitude above criticality. After lengthy calculations, it can be found that rolls are selected for thermal convection between two horizontal boundaries of high thermal heat conductivity [28], whereas a square pattern is preferred in the case of nearly insulating boundaries [29]. The selection mechanism results from the relative values of the coefficients of the nonlinear terms in the equations that govern the amplitudes $A_p(t)$ in the vicinity of the instability threshold. At the linear stage, the amplitude $A_p(t)$ displays an exponential growth or decay with the growth rate $\sigma_+(k, R) = \mu - \alpha(k - k_c)^2 + \dots = \mu$ for any p since \mathbf{k}_p has modulus k_c . The linear part of the equation for the amplitude $A_p(t)$ is therefore $\dot{A}_p = \mu A_p$. If the amplitudes remain small close to the instability threshold, we expect that the leading-order nonlinear terms give a correct description of the nonlinear dynamics and we look for an expansion of \dot{A}_p in powers of the A_q 's and their complex conjugates. If $N = 1$, there is only one amplitude A and all possible terms up to cubic order in the equation for \dot{A} are

$$A^2, A\bar{A}, \bar{A}^2, A^3, A^2\bar{A}, A\bar{A}^2, \bar{A}^3 \quad (21)$$

We observe that most of these terms cannot be involved in the amplitude equation because of symmetry constraints. As said above, the system is translationally invariant in the horizontal plane. Taking the x -axis along the wave vector \mathbf{k} of the pattern, the solution (20) with $N = 1$ spontaneously breaks translational invariance along the x -axis. However, if $w(x, z)$ is a solution to the problem, $w(x + x_0, z)$ with x_0 constant, is another solution. This new solution is obtained through the transformation $A \rightarrow A \exp(ik_c x_0)$. The amplitude equation should be invariant under this transformation, i.e. has rotational invariance in the complex plane. We find that only the term $A^2\bar{A}$ transforms like A and can be kept in the amplitude equation

$$\dot{A} = \mu A - \beta |A|^2 A \quad (22)$$

where β is a complex coefficient. However, the system being invariant by reflection $x \rightarrow -x$, a transformation that amounts to $A \rightarrow \bar{A}$ from (20), the amplitude equation should be invariant under the transformation $A \rightarrow \bar{A}$. Performing this transformation in (22) and taking the complex conjugate, we obtain, after identifying with (22), $\bar{\beta} = \beta$, thus β real. If $\beta < 0$, the leading order nonlinearity saturates the linear growth above instability threshold and the bifurcation is supercritical or continuous. Otherwise, the bifurcation is subcritical and higher order nonlinear terms should be computed in order to describe the saturation mechanism.

For squares, we have

$$w(x, y, z, t) = ([A_1 \exp(ik_c x) + c.c.] + [A_2 \exp(ik_c y) + c.c.]) \sin \pi z + \dots \quad (23)$$

where $A_1(t)$ and $A_2(t)$ are the complex amplitudes of the two sets of perpendicular rolls and *c.c.* stands for the complex conjugate of the previous expression. Using symmetry considerations, the amplitude equations read

$$\dot{A}_1 = \mu A_1 - [\beta |A_1|^2 + \gamma |A_2|^2] A_1 \quad (24)$$

$$\dot{A}_2 = \mu A_2 - [\gamma |A_1|^2 + \beta |A_2|^2] A_2 \quad (25)$$

It is easy to show that for $\mu > 0$, stationary squares ($|A_1| = |A_2|$) are stable when $|\gamma| < \beta$, i.e. when the cross-coupling nonlinear term is small enough so that the two sets of rolls weakly interact; when their interaction is too strong, more precisely when, $\gamma > \beta$, one of the two sets of rolls nonlinearly damps out the other, and rolls are the stable nonlinear state. For hexagons, we have

$$w(x, y, z, t) = \sum_{p=1}^3 [A_p \exp(i\mathbf{k}_p \cdot \mathbf{r}) + c.c.] \sin \pi z + \dots \tag{26}$$

with $|\mathbf{k}_p| = k_c$ and $\mathbf{k}_1 + \mathbf{k}_2 + \mathbf{k}_3 = 0$, and where the $A_p(t)$'s are the complex amplitudes of the three sets of rolls. Using symmetry considerations, the amplitude equations read

$$\dot{A}_l = \mu A_l + \epsilon \bar{A}_m \bar{A}_n - [\beta |A_l|^2 + \delta (|A_m|^2 + |A_n|^2)] A_l, \text{ and cyclic permutations of } (l, m, n) \tag{27}$$

In contrast to rolls or squares, a quadratic nonlinear term proportional to $\bar{A}_m \bar{A}_n$ is involved in the evolution equation for A_l in the case of hexagons. This term is the dominant nonlinearity and it makes the bifurcation subcritical. One could therefore expect that hexagons will be observed at the instability threshold in generic situations. This is the case of Bénard cells obtained with a bottom rigid boundary and a top free surface. However, this is not true for convection in the Boussinesq approximation with symmetric top and bottom boundaries. In that case, there is an additional reflection symmetry with respect to the horizontal mid-plane, called the Boussinesq symmetry, $x \rightarrow x, z \rightarrow 1 - z, \mathbf{v} \rightarrow -\mathbf{v}, \theta \rightarrow -\theta$, that amounts to $A \rightarrow -A$ such that quadratic nonlinearities are not allowed. Without quadratic nonlinearities, the stability domains of rolls, squares, and hexagons depend on the values of β, γ, δ , and μ .

Stripes, parallelograms, hexagons and triangles are the only periodic tiling of the plane. Values of N larger than 3 in (20) correspond to patterns with quasi-crystalline symmetries. They have rotational order, but no translational order. It has been shown that they can be generated at the instability threshold of the Faraday instability when the fluid layer is vibrated with two frequencies [30,31] or in the vicinity of some particular point in parameter space [32]. Time independent spatially random patterns also can be generated at the instability threshold [33]. It happens sometimes that no stationary pattern exists even immediately above a stationary instability onset; the nonlinear regime is then time-periodic or chaotic.

5.2. Finite range of unstable wavenumbers above the instability threshold

Another problem results from the existence of a continuous band of unstable modes above criticality, as described by Eq. (17). Linear analysis only determines the one with the highest growth rate ($k = k_c$), but the wavenumber selected by nonlinear interactions may correspond to a different one. The interaction of two (or several) modes within the unstable band gives rise to a spatial modulation of the periodic pattern on a large length scale compared to the pattern wavelength. The inverse of this length scale is in the order of $(k - k_c)$, which is small close to the instability threshold. In order to take into account this band of unstable wavenumbers, the idea is to consider a wave packet with a complex amplitude $A(x, t)$ slowly varying in space and time, and to find the partial differential equation that governs $A(x, t)$ close to the instability threshold. We consider the case of a one-dimensional pattern for simplicity and write

$$w(x, z, t) = [A(x, t) \exp(ik_c x) + c.c.] \sin \pi z + \dots \tag{28}$$

The linear part of the equation for A can be easily found as follows: we write

$$A(x, t) = \int \hat{A}(K, \sigma) \exp(\sigma t + iKX) \delta[\sigma - \sigma_+(K, \mu)] dK d\sigma \tag{29}$$

Equation (17) for the growth rate gives

$$\sigma_+ \hat{A}(K, \sigma) = \mu \hat{A}(K, \sigma) - \alpha K^2 \hat{A}(K, \sigma) + \dots \tag{30}$$

Taking the Laplace transform in time and the Fourier transform in space gives

$$\frac{\partial A}{\partial t} = \mu A + \alpha \frac{\partial^2 A}{\partial x^2} + \dots \tag{31}$$

The leading order nonlinear term can then be obtained by using symmetry arguments as done above. Using appropriate units of amplitude and space, we get

$$\frac{\partial A}{\partial t} = \mu A + \frac{\partial^2 A}{\partial x^2} - |A|^2 A \tag{32}$$

This equation has been found by Newell and Whitehead [34] and Segel [35] using the method of multiple scales. Multiplying Eq. (32) by $\partial A / \partial t$ and adding to the complex conjugate expression, we can check that there is a Lyapunov functional,

$$F[A, \bar{A}] = \int \left[\left| \frac{\partial A}{\partial x} \right|^2 - \mu |A|^2 + \frac{1}{2} |A|^4 \right] dx = \int \left[\left| \frac{\partial A}{\partial x} \right|^2 - V(|A|^2) \right] dx \quad (33)$$

such that

$$\frac{dF}{dt} = -2 \int \left| \frac{\partial A}{\partial t} \right|^2 dx < 0 \quad (34)$$

with $F[A, \bar{A}]$ bounded from below. The dynamics is of potential type in the vicinity of instability threshold

$$\frac{\partial A}{\partial t} = -\frac{\delta F}{\delta \bar{A}} \quad (35)$$

and the system tries to minimize $F[A, \bar{A}]$, which can be considered as some kind of free energy. This is achieved for homogeneous patterns with $|A|^2 = \mu$ above the instability threshold ($\mu > 0$). The pattern with wavenumber k_c is therefore the globally stable one.

We observe that F has the same form as the Ginzburg–Landau free energy for superconductivity (without taking into account the coupling with the electromagnetic field). Pattern-forming instabilities share a lot of analogies with phase transitions. In the case of the Rayleigh–Bénard instability, the order parameter is the complex amplitude A of the pattern, which grows like $\sqrt{\mu}$ above the instability threshold; the inverse of the instability growth rate is the time scale τ of A , which diverges at the threshold, $\tau \propto \mu^{-1}$, and there is a coherence length ξ of the spatial variations of A , which also diverges at the threshold, $\xi \propto \mu^{-1/2}$. These critical behaviors have been checked in experiments [36] and the mean field exponents have been precisely measured. Thermal fluctuations are indeed negligible at distances to threshold that can be studied in experiments.

We can go back to Bénard's concern about the effect of lateral boundaries on the convection patterns. Strictly speaking, the coherence length being infinite at instability threshold, lateral boundaries affect the pattern whatever the horizontal extension of the fluid layer. Therefore, if we manage to tune the Rayleigh number close enough to the threshold, the pattern consists of a linear mode of the container and is not selected by nonlinear interactions among many different unstable linear modes. In order to get many unstable linear modes slightly above threshold, the marginal stability curve should be very flat close to k_c , which means that α is small. If the horizontal extension L of the fluid layer is such that $L \gg \sqrt{\alpha} d$, the coherence length remains small compared to L at distances to threshold that can be studied in experiments and the lateral boundaries affect the pattern only in their vicinity, as observed by Bénard. The pattern is then selected by nonlinear interactions between linearly unstable modes.

We now consider stationary solutions to the amplitude equation in the form

$$A_q = Q \exp i q x \quad (36)$$

which represents patterns with wavelengths $k_c + q$. We get from (32),

$$Q^2 = \mu - q^2 \quad (37)$$

Therefore, all linearly unstable modes of wavenumber q of the solution $A = 0$ (such that $q^2 < \mu$ above threshold), give rise to a nonlinearly saturated stationary solution with amplitude $A_q = \sqrt{\mu - q^2} \exp i q x$. These solutions correspond to patterns with different wavenumbers $k_c + q$ with $-\sqrt{\mu} < q < \sqrt{\mu}$. These are the patterns with different wavelengths observed by Bénard and Avsec [5]. However, all the patterns with $q \neq 0$ have a larger free energy than the pattern with optimal wavenumber k_c . We will explain below why some of them are metastable and do not relax to the pattern with the lowest free energy.

5.3. Eckhaus instability

To study the linear stability of the solutions $A_q = \sqrt{\mu - q^2} \exp i q x$ of (32), we perturb their amplitude and phase, thus writing

$$A = [Q + r(x, t)] \exp (i q x + \phi(x, t)) \quad (38)$$

in Eq. (32). Expanding, separating real and imaginary parts and keeping only linear terms in r and ϕ yields

$$\frac{\partial r}{\partial t} = -2 Q^2 r + \frac{\partial^2 r}{\partial x^2} - 2 q Q \frac{\partial \phi}{\partial x} \quad (39)$$

$$\frac{\partial \phi}{\partial t} = 2 \frac{q}{Q} \frac{\partial r}{\partial x} + \frac{\partial^2 \phi}{\partial x^2} \quad (40)$$

We consider modes proportional to $\exp(\eta t + i K x)$ and get from Eq. (40) the dispersion relation which has solutions

$$\eta(K) = -(Q^2 + K^2) \pm \sqrt{Q^4 + 4K^2q^2} \quad (41)$$

Thus, for small K , we have two different branches:

- the “amplitude modes”, $\eta_-(K) = -2Q^2 + O(K^2)$, which are damped,
- the “phase modes”, $\eta_+(K) = -K^2(1 - 2q^2/Q^2) + O(K^4)$, which are marginal in the limit $K \rightarrow 0$. The phase modes

$$\eta_+(K) = -\frac{\mu - 3q^2}{\mu - q^2}K^2 - 2\frac{q^4}{(\mu - q^2)^3}K^4 + O(K^6) \quad (42)$$

lead to an instability when

$$D_{\parallel} = \frac{\mu - 3q^2}{\mu - q^2} < 0 \quad (43)$$

thus when $q^2 < \mu < 3q^2$; this is the Eckhaus instability.

The Eckhaus instability therefore restricts the band of wavenumbers $k_c + q$ of metastable patterns above threshold to values of q such that $q^2 < \mu/3$. These patterns are only linearly stable, i.e. stable to small perturbations. A transition to a pattern with a smaller q , i.e. with a lower free energy, can be induced by a finite amplitude perturbation. The Eckhaus instability is indeed subcritical. For $q^2 < \mu/3$, the energy barrier that should be crossed to destabilize the pattern can be computed using (32). It vanishes at the threshold of the Eckhaus instability. The metastable patterns with different wavelengths observed by Bénard and Avsec [5], and their instability when their wavelength deviates too much from the optimal wavelength can therefore be understood as the Eckhaus instability.

In the framework of the analogy with superconductivity, the Eckhaus instability is related to the critical current density needed to induce the transition from the superconducting state to the normal one.

5.4. Broken symmetries and secondary instabilities

When analyzing the linear stability of a periodic pattern generated by a stationary instability close to the threshold, we observed that whereas perturbations of the amplitude are damped in the long-wavelength limit, perturbations of the phase are marginal, i.e. have a vanishing growth rate in the limit $K \rightarrow 0$. This is related to the spontaneously broken translational invariance at the instability onset. Consider for instance a pattern of rolls along the x -axis generated by the Rayleigh–Bénard instability, i.e. a stationary solution $\mathbf{v}_0(x, z)$, $\pi_0(x, z)$, $\theta_0(x, z)$ of the Boussinesq equations. We consider

$$\mathbf{v}(x, z, t) = \mathbf{v}_0[x + \phi(t), z] \simeq \mathbf{v}_0(x, z) + \phi(t) \frac{\partial \mathbf{v}_0}{\partial x} \quad (44)$$

and similar expressions for π and θ . Substituting into (7), (8), we get

$$\frac{\partial \phi}{\partial t} = 0 \quad (45)$$

which shows that a homogeneous perturbation of amplitude $\phi(t)$ along $\partial \mathbf{v}_0 / \partial x$ has zero growth rate. In other words, push the roll structure without deformation along the x -axis, or equivalently change the origin of the x -axis, is a neutral perturbation that does not grow, neither decay. A neutral phase mode is related to the spontaneously broken translational symmetry at the instability onset. If we now consider inhomogeneous perturbations of the form $\phi(x, t)$ with ϕ slowly varying in x on a length scale large compared to the wavelength of the pattern, we can expect that the zero growth rate at $K = 0$ could become positive for $K > 0$ and lead to a secondary instability of the pattern. This is precisely what occurs for the Eckhaus instability. Secondary instabilities related to modes that trace back to spontaneously broken symmetries at the primary instability onset are called phase instabilities [37–39]. They are the analogues of Goldstone modes in field theory or condensed-matter physics.

Nonlinear evolution equations for phase modes can be found using symmetry arguments. Translational invariance along the x -axis implies that the phase equation should be invariant under the transformation $x \rightarrow x + x_0$, $\phi \rightarrow \phi + x_0$; therefore, all terms with explicit dependence on ϕ are forbidden in the equation for $\partial \phi / \partial t$. Reflection symmetry forces the phase equation to be invariant under the transformation $x \rightarrow -x$, $\phi \rightarrow -\phi$; therefore, the number of occurrences of ϕ and $\partial / \partial x$ in each term of the phase equation should be odd. This gives to the leading order

$$\frac{\partial \phi}{\partial t} = D_{\parallel} \frac{\partial^2 \phi}{\partial x^2} - \kappa_{\parallel} \frac{\partial^4 \phi}{\partial x^4} + g_{\parallel} \frac{\partial \phi}{\partial x} \frac{\partial^2 \phi}{\partial x^2} \quad (46)$$

We need $\kappa_{\parallel} > 0$ in order to have stability at short wavelength. It can be shown that the leading-order nonlinear term does not saturate the instability when $D_{\parallel} < 0$, i.e. the Eckhaus instability is subcritical.

The same analysis can be performed for a transverse phase perturbation $\phi(y, t)$ of the roll pattern along the x -axis, like the one displayed in Fig. 4. We get

$$\frac{\partial \phi}{\partial t} = D_{\perp} \frac{\partial^2 \phi}{\partial y^2} - \kappa_{\perp} \frac{\partial^4 \phi}{\partial y^4} + g_{\perp} \left(\frac{\partial \phi}{\partial y} \right)^2 \frac{\partial^2 \phi}{\partial y^2} \quad (47)$$

We observe that, in contrast to the Eckhaus instability, the leading order nonlinear term can compensate $D_{\perp} < 0$ when the phase gradient is large enough and saturates the growth if $g_{\perp} > 0$. In that case, the sinuous or “zigzag” instability of convection rolls is supercritical.

More complex phase dynamics occur when there exist additional symmetries that are broken at the instability onset. For instance, broken Galilean invariance makes the dynamics second order in time such that oscillatory phase instabilities that amplify wavy modes of the pattern are observed [40]. In the case of a primary standing-wave pattern, there are two phase modes related to broken translational invariance in space and time, respectively. These modes are nonlinearly coupled, such that the phase instability comes in at finite wavenumber instead of $K \rightarrow 0$ [41].

5.5. Spontaneously broken chirality and drifting patterns

All the secondary instabilities of periodic patterns are of course not phase instabilities, but phase modes are likely to play an important role in all cases. A widely observed class of secondary instabilities of a periodic pattern are “drift instabilities” [42]. After a first bifurcation to a stationary cellular structure, $\mathbf{v}_0(x, z)$, further increase in the bifurcation parameter generates a secondary bifurcation to a traveling pattern of the form $\mathbf{v}_D(x \pm ct, z)$. The motion of the pattern in one of the preferential directions, $\pm x$, breaks the space reflection symmetry. The amplitude V of the drift bifurcation could be related to the difference between twice the phase of the pattern and the phase of its second harmonic in the case of a stationary pattern or to the difference between the amplitudes of the two counter-propagating waves of a standing wave pattern [43]. In the vicinity of this instability onset, we write

$$\mathbf{v}(x, z, t) = \mathbf{v}_0[x + \phi(x, t), z] + V(x, t) \mathbf{v}_{\pi}(x, z) + \dots \quad (48)$$

where $\mathbf{v}_{\pi}(x, z)$ is the eigenmode of the instability. In the absence of phase modes, we assume that reflection symmetry is broken by a supercritical pitchfork bifurcation with amplitude equation

$$\frac{\partial V}{\partial t} = \lambda V - V^3 \quad (49)$$

where λ is the eigenvalue that vanishes at instability threshold. The drift instability results from the coupling between the reflection symmetry-breaking amplitude mode V and the phase mode ϕ associated with translational invariance. Coupled equations for ϕ and V are constrained by the symmetries $x \rightarrow x + x_0$, $\phi \rightarrow \phi + x_0$ and $x \rightarrow -x$, $\phi \rightarrow -\phi$, $V \rightarrow -V$. We get

$$\frac{\partial \phi}{\partial t} = V \quad (50)$$

$$\frac{\partial V}{\partial t} = \lambda V - V^3 + a \frac{\partial^2 \phi}{\partial x^2} + b \frac{\partial^2 V}{\partial x^2} + f V \frac{\partial \phi}{\partial x} + g V \frac{\partial V}{\partial x} + h \frac{\partial \phi}{\partial x} \frac{\partial^2 \phi}{\partial x^2} \quad (51)$$

Higher-order terms in the first equation can always be removed via a nonlinear transformation [43] and the coefficient in front of V has been scaled in V . If the coefficients, a, b are positive, the $V = 0$ solution first bifurcates when λ vanishes and becomes positive. The homogeneous drifting pattern, $V_0 = \pm\sqrt{\lambda}$, $\phi_0 = V_0 t$, bifurcates supercritically and the sign of the selected solution for V determines the direction of propagation of the pattern. However, for modulated patterns in space, the term $fV \partial \phi / \partial x$ destabilizes the homogeneous pattern whatever the sign of f and is the dominant nonlinear term. It makes the bifurcation subcritical and solutions that consist of localized drifting regions with tilted cells exist before the onset of the homogeneous drift bifurcation [44]. Other examples where coupling with phase modes make a transition first order have been reported [45]. A similar mechanism could also affect the Peierls transition.

6. Concluding remarks

Bénard’s work was not understood by most of his colleagues. Originality is acknowledged to some extent in the examiners’ report on his thesis, but this report also states that Bénard could have performed much better. After Bénard’s death, the new director of the laboratory answered students who were inquiring whether it would be possible to carry out a PhD work on Bénard’s topics that these topics were exhausted [11]. However, Bénard’s experiments directly motivated Rayleigh and others in their theoretical work on stability analysis in fluid dynamics and were well recognized abroad.

Bénard was a precursor in many respects: besides his pioneering study on pattern-forming instabilities, he was one of the first to conduct research in fluid mechanics using quantitative measurements with state of the art techniques. He used cinematography not only as a measurement technique, but also to present science to a general audience. He also performed laboratory experiments in order to get insight into phenomena occurring in astrophysics or meteorology decades before this became commonplace. Pattern-forming instabilities became a very active topic of research in the 1970s, and a lot of experimental as well as theoretical work was performed in the spirit of Bénard’s first experiments.

References

- [1] H. Bénard, *Etude expérimentale du mouvement des liquides propageant la chaleur par convection. Régime permanent: tourbillons cellulaires*, C. r. hebdomadaire des séances Acad. sci. Paris 130 (1900) 1004–1007.

- [2] H. Bénard, Mouvements tourbillonnaires à structure cellulaire. Etude optique de la surface libre, C. r. hebd. séances Acad. sci. Paris 130 (1900) 1065–1068.
- [3] M. Faraday, On the forms and states assumed by fluids in contact with vibrating elastic surfaces, Philos. Trans. R. Soc. Lond. 52 (1831) 319–340.
- [4] W. Thomson, Hydrokinetic solutions and observations, Philos. Mag. 42 (1871) 362–377.
- [5] H. Bénard, D. Avsec, Travaux récents sur les tourbillons cellulaires et les tourbillons en bandes. Applications à l'astrophysique et à la météorologie, J. Phys. Radium 9 (1938) 486–500.
- [6] E.A. Spiegel, Convection in stars, Annu. Rev. Astron. Astrophys. 9 (1971) 323–352; 10 (1972) 261–304.
- [7] E. Palm, Nonlinear thermal convection, Annu. Rev. Fluid Mech. 7 (1975) 39–61.
- [8] C. Normand, Y. Pomeau, M.G. Velarde, Convective instability: a physicist approach, Rev. Mod. Phys. 49 (1977) 581–624.
- [9] F.H. Busse, Nonlinear properties of convection, Rep. Prog. Phys. 41 (1978) 1929–1967.
- [10] F.H. Busse, Transition to turbulence in Rayleigh–Bénard convection, in: H.L. Swinney, J.P. Gollub (Eds.), Hydrodynamic Instabilities and the Transition to Turbulence, 2nd edition, in: Topics in Applied Physics, vol. 45, Springer, Berlin, 1985, pp. 97–137.
- [11] J.E. Wesfreid, Scientific biography of Henri Bénard (1874–1939), in: I. Mutabazi, J.E. Wesfreid, E. Guyon (Eds.), Dynamics of Spatio-Temporal Cellular Structures, in: Springer Tracts in Modern Physics, vol. 207, Springer, New York, 2006, pp. 9–37.
- [12] H. Bénard, Les tourbillons cellulaires dans une nappe liquide transportant de la chaleur par convection en régime permanent, Ann. Chim. Phys. 23 (1901) 62–144.
- [13] H. Bénard, Formation périodique de centres de giration à l'arrière d'un obstacle en mouvement, C. r. hebd. séances Acad. sci. Paris 147 (1908) 839–842.
- [14] H. Bénard, Etude cinématographique des remous et des rides produits par la translation d'un obstacle, C. r. hebd. séances Acad. sci. Paris 147 (1908) 970–972.
- [15] L. Rayleigh, On convection currents in a horizontal layer of fluid, when the higher temperature is on the under side, Philos. Mag. Ser. 6 32 (1916) 529–546.
- [16] J. Boussinesq, Théorie analytique de la chaleur, vol. II, Gauthier-Villars, Paris, 1903.
- [17] A. Pellew, R.V. Southwell, On maintained convective motion in a fluid heated from below, Proc. R. Soc. A 176 (1940) 312–343.
- [18] D.T.J. Hurle, E. Jakeman, E.R. Pike, On the solution of the Bénard problem with boundaries of finite conductivity, Proc. R. Soc. Lond. A 296 (1967) 469–475.
- [19] H. Bénard, Sur les tourbillons cellulaires et la théorie de Rayleigh, C. r. hebd. séances Acad. sci. Paris 185 (1927) 1109–1111.
- [20] C. Dauzère, Sur la stabilité des tourbillons cellulaires, C. r. hebd. séances Acad. sci. Paris 154 (1912) 974–977.
- [21] V. Volkoviski, Sur les tourbillons en festons, C. r. hebd. séances Acad. sci. Paris 200 (1935) 1285–1287.
- [22] M.J. Block, Surface tension as the cause of Bénard cells and surface deformation in a liquid film, Nature 178 (1956) 650–651.
- [23] J.R.A. Pearson, On convection cells induced by surface tension, J. Fluid Mech. 4 (1958) 489–500.
- [24] P. Idراع, Sur les courants de convection dans l'atmosphère dans leur rapport avec le vol à voile et certains types de nuages, C. r. hebd. séances Acad. sci. Paris 171 (1920) 42–44.
- [25] H. Journaud, Sur les tourbillons en bandes, C. r. hebd. séances Acad. sci. Paris 194 (1932) 52–53.
- [26] D. Avsec, Sur les formes ondulées des tourbillons en bandes longitudinales, C. r. hebd. séances Acad. sci. Paris 204 (1937) 167–169.
- [27] V. Volkoviski, Sur les tourbillons en bandes dans les liquides, C. r. hebd. séances Acad. sci. Paris 204 (1937) 1461–1463.
- [28] A. Schlüter, D. Lortz, F. Busse, On the stability of steady finite amplitude convection, J. Fluid Mech. 23 (1965) 129–144.
- [29] F.H. Busse, N. Riahi, Nonlinear convection in a layer with nearly insulating boundaries, J. Fluid Mech. 90 (1980) 243–250.
- [30] W.S. Edwards, S. Fauve, Structure quasicristalline engendrée par instabilité paramétrique, C. R. Acad. Sci. Paris, Ser. II 315 (1992) 417–420.
- [31] W.S. Edwards, S. Fauve, Patterns and quasi-patterns in the Faraday experiment, J. Fluid Mech. 278 (1994) 123–148.
- [32] D. Binks, W. van de Water, Nonlinear pattern formation of Faraday waves, Phys. Rev. Lett. 78 (1997) 4043–4046.
- [33] A.C. Newell, Y. Pomeau, Turbulent crystals in macroscopic systems, J. Phys. A 26 (1993) L429–L434.
- [34] A.C. Newell, J.A. Whitehead, Finite bandwidth, finite amplitude convection, J. Fluid Mech. 38 (1969) 279–303.
- [35] L.A. Segel, Distant side-walls cause slow amplitude modulation of cellular convection, J. Fluid Mech. 38 (1969) 203–224.
- [36] J. Wesfreid, Y. Pomeau, M. Dubois, C. Normand, P. Bergé, Critical effects in Rayleigh–Bénard convection, J. Phys. France 39 (1978) 725–731.
- [37] Y. Kuramoto, T. Tsuzuki, Persistent propagation of concentration waves in dissipative media far from thermal equilibrium, Prog. Theor. Phys. 55 (1976) 356–369.
- [38] Y. Pomeau, P. Manneville, Stability and fluctuations of a spatially periodic convective flow, J. Phys. Lett. 40 (1979) 609–612.
- [39] Y. Kuramoto, Phase dynamics of weakly unstable periodic structures, Prog. Theor. Phys. 71 (1984) 1182–1196.
- [40] P. Couillet, S. Fauve, Propagative phase dynamics for systems with Galilean invariance, Phys. Rev. Lett. 55 (1985) 2857–2860.
- [41] P. Couillet, S. Fauve, E. Tirapegui, Large scale instability of nonlinear standing waves, J. Phys. Lett. 46 (1985) 787–791.
- [42] P. Couillet, R.E. Goldstein, G.H. Gunaratne, Parity-breaking transitions of modulated patterns in hydrodynamic systems, Phys. Rev. Lett. 63 (1989) 1954–1957.
- [43] S. Fauve, S. Douady, O. Thual, Drift instabilities of cellular patterns, J. Phys. II 1 (1991) 311–322.
- [44] B. Caroli, C. Caroli, S. Fauve, On the phenomenology of tilted domains in lamellar eutectic growth, J. Phys. I 2 (1992) 281–290.
- [45] T. Dessup, C. Coste, M. Saint Jean, Subcriticality of the zigzag transition: a nonlinear bifurcation, Phys. Rev. E 91 (2015) 032917.